Available online at www.sciencedirect.com
ScienceDirect
Journal of Power Sources 171 (2007) 310–320
JOURNAL OF POWER SOURCES
www.elsevier.com/locate/jpowsour

From macro- to micro-single chamber solid oxide fuel cells

B.E. Buergler, M. Ochsner, S. Vuillemin, L.J. Gauckler *

Department Materials, ETH Zurich, 8093 Zurich, Switzerland

Received 11 August 2006; received in revised form 31 May 2007; accepted 17 June 2007
Available online 30 June 2007

Abstract

Single chamber solid oxide fuel cells (SC-SOFCs) with interdigitating electrodes were prepared and operated in CH_4/air mixtures. Both electrodes (Ni-$Ce_{0.8}Gd_{0.2}O_{1.9}$ cermet and $Sm_{0.5}Sr_{0.5}CoO_{3-\delta}$ perovskite) were placed on the same side of a $Ce_{0.8}Gd_{0.1}O_{1.95}$ electrolyte disc. The separating gap between the electrodes was varied from 1.2 to 0.27 mm and finally down to 10 μm. Screen-printing was used for the preparation of the cells with a gap in the millimetre range, whereas micromolding in capillaries (MIMIC) was used for the preparation of the micro-SC-SOFCs.

The prepared micro-SC-SOFCs consisted of an array of 19 individual cells that were connected in parallel having 100 μm wide electrodes. An open circuit voltage of 0.65–0.75 V was measured in flowing mixtures of methane and air. The maximum power density of 17 mW cm^{-2} was limited by the ohmic resistance of the long conduction paths along the thin electrodes to the active sites of the individual cells. The feasibility of the micro-cell was demonstrated by comparing the performance with the performance of the cells having feature sizes in the millimetre range. The cell resistance of micro-SC-SOFCs may be significantly reduced when connecting the cells in series using interconnections between anode and cathodes of adjacent cells.

Keywords: Ceramic materials; Single chamber; Solid oxide fuel cell; Micromolding in capillaries; Micro-cell

1. Introduction

In 1965, van Gool proposed a novel fuel cell design using surface-migration of ions on a solid electrolyte in mixtures of fuel and air [1], and a similar invention was patented by Louis in 1981 [2]. This new type of electrochemical cell in hydrogen air mixtures comprised laterally spaced side by side catalyst layers as electrodes with a gap between the catalysts being bridged by a solid electrolyte. The concept of single chamber solid oxide fuel cells (SC-SOFCs) operating at temperatures above 500 °C was demonstrated in practice for the first time by Hibino and Iwahara [3]. In the single chamber configuration, there is only one gas compartment, thus the electrodes can be placed beside each other on the same electrolyte surface, whereas in conventional SOFCs the electrodes are placed on opposite sides. It has been shown that the side by side cell design can generate an open circuit voltage (OCV) and that the ohmic resistance of the cell decreased as the gap between the electrodes became smaller [4]. The possibility to easily interconnect individual cells on one and the same electrolyte disc was pointed out. Two series connected cells on the same substrate made of yttria-stabilised zirconia (YSZ) showed an OCV that was twice as high as the OCV of a single cell. On the other hand, two cells connected in parallel exhibited only half of the resistance. Cells with a gap width of 1 mm that were operated at 950 °C in methane–air mixtures yielded a power output in the range of 45 mW cm^{-2}. By keeping the YSZ substrate, but using $La_{0.8}Sr_{0.2}MnO_3$ and $Ce_{0.8}Gd_{0.2}O_{1.9}$-containing nickel cermet as cathode and anode, respectively, the performance of the cells with the same geometry could be improved to 120 mW cm^{-2} [5] as compared to 45 mW cm^{-2} [4] obtained with metallic electrodes. Ceria-based electrolytes allowed for a drastic reduction of the operating temperature. Cells with $Ce_{0.8}Gd_{0.2}O_{1.90}$-electrolyte (CGO) showed an OCV of about 800 mV and a maximum power density of 122 mW cm^{-2} at 500 °C [6]. At this temperature the ceria solid solution is primarily an ionic conductor even at an oxygen partial pressure ($p(O_2)$) of down to 10^{-25} atm [7].

Hibino et al. proposed a new cell design with interpenetrating comb-like electrode patterns on the same surface of an electrolytic material having feature sizes in the millimetre range

* Corresponding author. Tel.: +41 44 6325646; fax: +41 44 6321132.
E-mail address: ludwig.gauckler@mat.ethz.ch (L.J. Gauckler).

0378-7753/$ – see front matter © 2007 Elsevier B.V. All rights reserved.
doi:10.1016/j.jpowsour.2007.06.204

[8], which has not yet been experimentally validated. The questions, which shapes, geometries, electrochemical properties of the electrodes and which electrolyte thickness are required to obtain an optimal performance was addressed by Fleig et al. in a recent modelling publication [9]. For interpenetrating comb-like structures of anode and cathodes, the cells would have to have electrodes with characteristic feature sizes of a few micrometres. However, it has not been proven that a cell with a very small gap between the anode and the cathode can give a reasonable OCV. It is possible that the reaction products of the partial oxidation of a hydrocarbon from the anode can easily reach the cathode, thereby suppressing the oxygen partial pressure at the cathode and consequently the OCV.

Chung and Chung carried out finite element modelling of a micro-SC-SOFC with side by side design [10]. Cells with ceria electrolyte, NiO-CGO anode and SSC cathode were modelled. The results of this work showed that the resistance of the cell could be decreased by increasing the electrolyte thickness and by decreasing the gap width between the anode and cathode. However, the paper ignored the fact that the SC-SOFC operation is based on the partial oxidation of a hydrocarbon, as shown by Hibino and Iwahara [3]. Furthermore, hydrogen–air mixtures were assumed as well as perfectly selective electrodes resulting in OCV values of 1.13 V. Experiments with similar cells in CH_4–air mixtures gave OCVs of only around 0.9 V [11]. With an electrode spacing of 20 μm at a temperature of 500 °C, the cell with 20 μm wide and 20 μm high electrodes was calculated to yield a power output in the range of 100 mW cm^{-2} [10].

The aim of this study was to demonstrate the concept of the side by side design with electrode widths and spacings in the micrometre range and to develop a suitable process for the preparation of these micro-SC-SOFCs. Promising techniques can be found in the domain of soft lithography that allows the deposition of polymers and ink molecules onto various substrates [12,13]. It has been shown that it is possible to adopt the soft lithography technique to ceramics by using ceramic suspensions [14,15]. By micromolding in capillaries (MIMIC), which is one of the soft lithography techniques, Heule and Gauckler were able to fabricate porous SnO_2-microlines [16], which could be used as sensor arrays [17] for miniaturised gas sensors. The electrodes of a micro-SC-SOFCs would have to be quite similar to these microlines in terms of dimensions and structure. But in order to fabricate alternating lines of anode and cathode material for micro-SC-SOFCs, a modified MIMIC process had to be developed. By filling closed-end capillaries from opposite sides of a PDMS-mold with suspensions containing the anode and cathode materials, both electrodes can be fabricated in one single step. No tedious aligning has to be done for the preparation of anode and cathode microlines being separated by a very narrow gap of a few micrometres. The gas permeability of the polydimethylsiloxan (PDMS)-mold [18] allows filling microchannels that are closed at one end. The proposed process inherently produces cells that are connected in parallel by the electrode material deposited at the entrance of the capillaries. If the cells were to be connected in series, the preparation of interconnection lines between the anodes and the cathodes of neighbouring cells would have to be done and an additional aligning step would be required.

The performance of the micro-SC-SOFCs was compared with the performance of cells with electrode dimensions and spacings in the millimetre range. These cells with side by side design were fabricated in a similar way as previously described [19] by screen-printing the electrode layers. Four parallel-connected cells were also prepared having the same design as the micro-SC-SOFCs but with electrodes being 10 times wider and the gap width being more than 35 times larger. The voltage–current characteristics of the prepared cells were measured in methane–air mixtures then compared with each other. In order to obtain the specific power output of the cells, the electric current was divided, not by the area of a single electrode, but by the total area of the cell including the area of the spacings between the electrodes.

2. Experimental

2.1. Powders

The powders that were used for the preparation of SC-SOFCs are summarised in Table 1. The average particle size was estimated from the specific surface area (SSA) that was measured by N_2-adsorption (BET). The densities of the powders were measured by helium pycnometry with an accuracy of ± 0.01 g cm^{-3}.

2.2. Electrolyte pellets

Electrolyte discs were fabricated by uniaxially pressing 7 g of $Ce_{0.9}Gd_{0.1}O_{1.95}$ (CGO, Rhodia, Catalysis & Electronics, France) powder with an average particle size of 22.9 nm (measured by BET) in a 30 mm diameter dye at 40 MPa. The discs were then isostatically pressed at 300 MPa and sintered at 1400 °C in air for 2 h. A heating rate of 1 K min^{-1} and a cooling rate of 5 K min^{-1} were applied. In order to obtain flat surfaces, the sintered discs were lapped on a Stähli FLM 500 lapping machine equipped with a hybrid copper–steel disc. B_4C-suspension (BC-800, Stähli Switzerland) was used at 60 rpm and about one drop of B_4C-suspension every second. The density of the discs was measured after lapping and exceeded 97% of the theoretical density (ρ_{th} = 7.29 g cm^{-3}).

Table 1
Powders used for the preparation of SC-SOFCs

Powder	Function	Supplier	SSA (m^2 g^{-1})	Particle size (nm)	Density (g cm^{-3})	Lot no.
$Ce_{0.9}Gd_{0.1}O_{1.95}$ (CGO10)	Electrolyte	Rhodia	35.84	22.9	6.64	9804401
$Sm_{0.5}Sr_{0.5}CoO_{3-\delta}$ (SSC)	Cathode	Nextech	5.46	336	6.53	91-82
NiO-CGO (60-40)	Anode	SSC	13.52	60.1	6.79	03_P1464BM

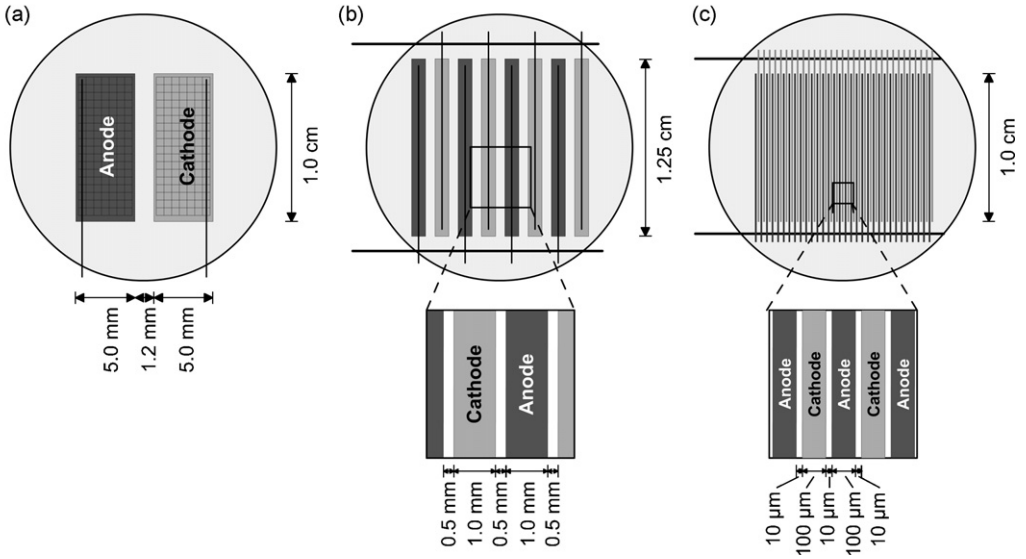

Fig. 1. Dimensions of the prepared side by side single chamber solid oxide fuel cells (SC-SOFCs). Macro-cell with 0.5 cm wide electrodes separated by a gap of 1.2 mm. (b) Milli-cell with four parallel-connected cells with electrode lengths and widths of 12.5 and 1 mm. (c) Micro-cell with electrode lengths and widths of 1 cm and 100 μm. The gap between the electrodes is 10 μm wide.

2.3. Cell designs

All the prepared cells had the side by side placement of electrodes with varying electrode and gap dimensions. On the one hand, cells with electrodes in the millimetre range were prepared; on the other, cells with micrometer-sized electrodes. The macro-cell shown in Fig. 1a had an electrode size of $0.5 \times 1.0\,cm^2$ with 1.2 mm spacing between the anode and the cathode. The milli-cell had eight electrodes, each with a size of $0.1 \times 1.25\,cm^2$ and an intracellular spacing of about 0.25 mm. The micro-cell design (Fig. 1c) had a total of 92 electrodes, each with $0.01 \times 1.0\,cm^2$ and a spacing of 10 μm between all electrodes. Pt-mesh and wire was used as the current-collectors for all the cells.

2.4. Preparation of macro-cells

The preparation steps for the macro-cell are depicted in Fig. 2. Both anode and cathode ($0.5 \times 1.0\,cm^2$) were similarly deposited in a side by side configuration by screen-printing them onto the electrolyte disc. A mask of 50 μm thickness was used in combination with suitable organic pastes. A 60 wt% NiO-containing $Ce_{0.8}Gd_{0.2}O_{1.9}$ (SSC, Salt Lake City, USA) was used as the anode and $Sm_{0.5}Sr_{0.5}CoO_{3-\delta}$ (Nextech Materials, Worthington, USA) as the cathode (see Table 1). Current-collectors were made by point welding Pt-wire onto a completely flat Pt-mesh $0.5 \times 1\,cm^2$ in size (52 mesh woven from 0.1 mm wire, Alfa Aesar). The current-collector was placed on the freshly printed layer, which was subsequently dried. The anode was

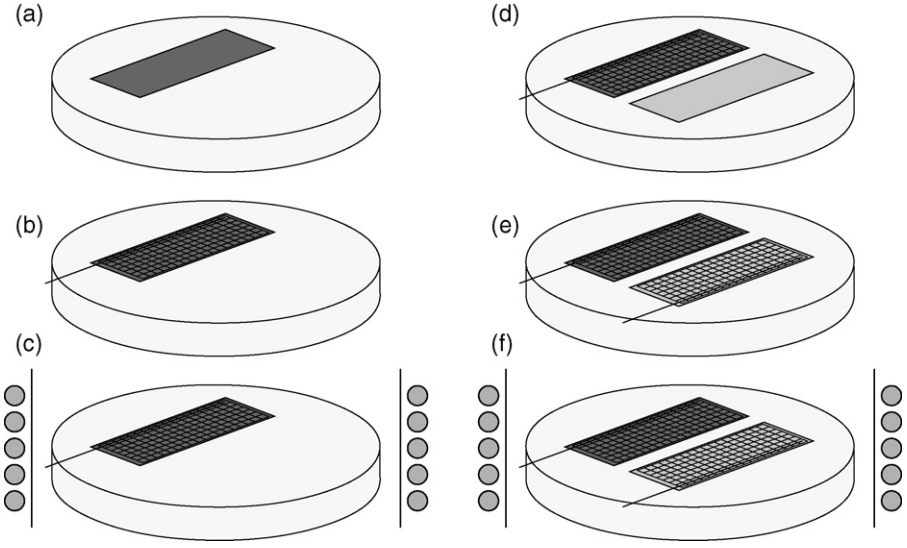

Fig. 2. Preparation of macro-cells. (a) Screen-print anode onto ion-conducting CGO substrate, (b) place current-collector on the anode layer, (c) sinter anode together with current-collector; (d) screen-print cathode beside anode, (e) place current-collector on cathode layer, (f) sinter cathode layer: macro-cell with feature sizes in the range of millimetres.

printed and sintered first (Fig. 2a–c), and then the cathode was prepared in a very similar manner as shown in Fig. 2d and e. Both electrodes were sintered at 1200 °C for 1 h in air. The heating rate was 1 K from room temperature to 500 °C with a dwell time of 1 h at this temperature and 3 K min^{-1} from there to the peak temperature. The samples were cooled down to room temperature at 5 K min^{-1}. Digital photographs of the prepared cell before and after the measurement are shown in Fig. 6.

2.5. Preparation of milli-cells

The preparation steps of milli-cell with four parallel-connected cells are depicted in Fig. 3. The cells had eight electrodes that were 12.5 mm × 1 mm in size. Therefore, the total electrode area was 1 cm^2; the cell area including inter-cellular (between neighbouring cells) as well as intracellular (within cells) gaps was 1.41 cm^2. In a first step, four anode strips were screen-printed through a mask of 50 μm thickness, which were subsequently sintered in the same way as described in Section 2.4, but with a peak temperature of 1300 °C (Fig. 3a and b). After that the cathode layers were printed (Fig. 3c) through the same mask forming an average intracellular gap of 0.27 mm and a gap between the electrodes of adjacent cells of 0.37 mm. After screen-printing, the edges of the electrodes spread out a little so that the final electrode width for both electrodes was about 1.1 mm. Flat Pt-wires that had been covered with the organic pastes of either the anode or cathode material were placed on the corresponding electrodes, and then sintering with a peak temperature of 1100 °C was done (Fig. 3d and e). Finally, the four anode and cathode contacts were point-welded each to a single piece of Pt-wire (Fig. 3f).

2.6. Preparation of micro-cells

2.6.1. Cathode and anode powders

The commercial $Sm_{0.5}Sr_{0.5}CoO_{3-\delta}$ powder (Nextech Materials, Worthington, USA) had a bimodal particle size distribution. A certain fraction of particles was larger than 2 μm, which is critical for the MIMIC process because the microchannels were only 7 μm in height. This fraction of large particles was removed by sedimentation of a well desagglomerated and stabilised suspension in a glass tube of 4 m length for 10 days. After this time, the large particles had sedimented at the bottom of the glass tube leaving behind the supernatant with fine particles, which was removed from the tube and dried. Only this powder fraction was used for preparing micro-cells. The large particles had been successfully removed by the sedimentation step. After sedimentation, the average particle size was 0.30 μm.

Commercial powder of 60 wt% NiO-containing $Ce_{0.8}Gd_{0.2}O_{1.9}$ (SSC, Salt Lake City, USA) was used as anode material. The primary particles were 50–200 nm in size but formed agglomerates with a diameter of up to 50 μm that had to be destroyed before the material could be used. This was done in a vibratory mill (Retsch MM 200) at a frequency of 20 Hz for 20 min. The anode powder had an average grain size of 60 nm, which allowed to sinter it a relatively low temperature of around 1100–1300 °C.

2.6.2. Suspensions for micromolding in capillaries

The most important parameters for a suitable suspension are the particle size, solid loading, the properties of the solvent and the wettability on the PDMS material and the CGO substrate. The capillaries of the PDMS-mold are only 7 μm high and if there are particles or agglomerates in the suspension being larger than that they will block the entrance of the capillaries and stop

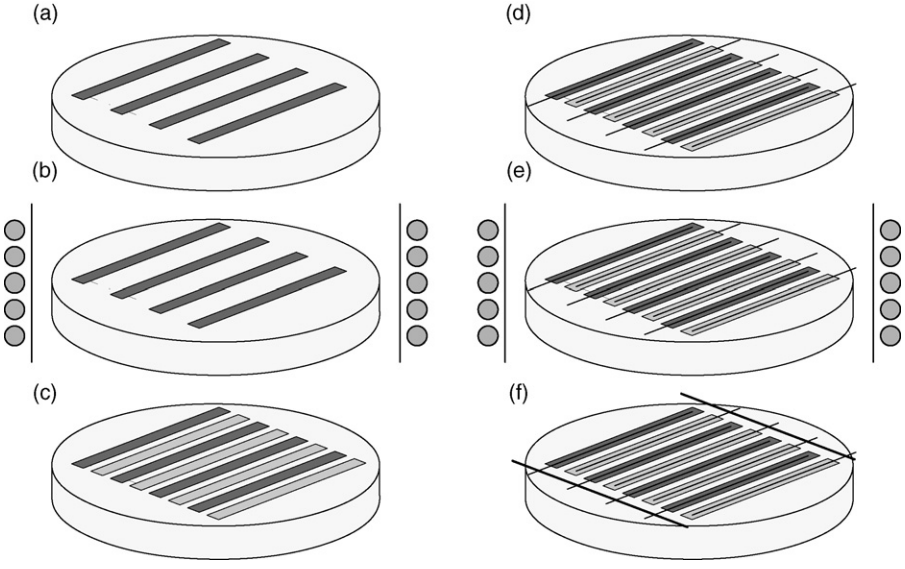

Fig. 3. Preparation of the milli-cell consisting of four parallel-connected cells. (a) Screen-print four anode strips in a single step, (b) sinter anodes, (c) print cathode strips, (d) place current-collectors on electrodes, (e) sinter electrodes with current-collectors, (f) point weld the cathode contacts and the anode contacts each to a piece of Pt-wire.

the filling process. Thus, powders must be used with a particle size smaller than about 1 μm and the suspensions must be thoroughly desagglomerated. The solid loading of the suspension must be as high as possible to avoid excessive drying shrinkage and to obtain thick and continuous electrodes. But if it is too high, the increased viscosity will impede the filling of the capillaries. The influence of solid loading of the used suspensions on the lines was studied by Heule [17]. The solvent is another very important parameter. With ethanol, the MIMIC process cannot work at ambient conditions because the drying is too fast. Neither could diethylene glycol monobutyl ether acetate with much slower drying rate be used because it swelled the PDMS-mold and led to detachment of the mold from the substrate. Aqueous suspensions of both powders were used in this study. Water was mixed with polyacrylic acid sodium salt (PAA; Molecular weight 2000 g mol^{-1}, Aldrich) such that the amount of PAA amounted to 1 wt% of the powder. Then the ceramic powder was added and the formed suspension homogenised by ultrasonification under stirring for 10 min. The suspensions were brought to pH 9 by adding ammonia (25% in H_2O) and were stable for several days without stirring. Different solid loadings were evaluated. For too low solid content, no material is deposited in the microchannels, while for too high solid loading the capillaries cannot be filled because the slurry is too viscous. Cathode and anode suspensions with 13 and 23 vol% of solid material, respectively, exhibited suitable properties for the filling of microchannels.

2.6.3. Preparation of the micromold

The master for the PDMS-molds was a photolithographically structured photo resist (AZ 4562, Clariant, Inc., Wiesbaden, Germany) covered silicon test grade wafer. Prebaking of the resist was performed on a hot plate for 3 min at 90 °C. The exposure of the 7-μm thick photo resist was done by a mask aligner (Suss MA-6) and the structures were developed in a mixture of Shipley developer 251 and water (1:3).

For the fabrication of the PDMS-molds, the structured wafer was placed in a Petri dish and covered with a 10/1 mixture of PDMS prepolymer/catalyst (Dow Corning, Inc., Midland, MI) under flow box conditions. The PDMS was cured for 2 h at 60 °C. Then the mold was carefully peeled off and two reservoirs for the suspensions were cut into the PDMS to open the ends of the capillaries on the two sides. After immersion in *n*-hexane for 60 min for removing non-reacted monomers, the PDMS-mold was oxygen-plasma-treated for 2 min in a Harrick PDC-32G steriliser. This turned out to be very important especially for aqueous suspensions of the electrode materials. In Table 2, the contact angles θ of water on PDMS and CGO are summarised before and after the plasma treatment. It is clear that without plasma-treatment, the MIMIC process could not have been done due to the microchannels being non-wetting. The filling of the capillaries would have been impossible. Because of 48% of the microchannels surface being CGO, it was of great importance to carry out the plasma cleaning also with the CGO substrate.

2.6.4. Micromolding in capillaries

All the steps for the fabrication of micro-cells are schematically shown in Fig. 4. First the PDMS-mold was placed on the CGO substrate and 20 μl of each suspension was filled into each reservoir (Fig. 4a and b). The filling of closed end capillaries was possible but at a rate that was more than hundred times slower than in the case of open-end channels. The reason for this was the increasing pressure of the air trapped in the capillary as the channels were being filled. Therefore, the filling process was limited by the air permeability of the PDMS-mold. The diffusion rate of air through the mold is proportional to the pressure difference across the PDMS and inversely proportional to the surface area of the capillary and the thickness of the mold. The filling velocity of the channels was in the range of 50 μm s^{-1} as was observed by microscopy. The adhesion of PDMS on CGO substrates was sufficient to perform the MIMIC process. After filling of the capillaries (Fig. 4c), the reservoirs were emptied (Fig. 4d) and sealed by adhesive tape in order to avoid too fast drying of the suspensions. Drying the green electrodes was problematic when the material in the reservoir dried before the material in the capillary did. Then, through capillary forces of the powder in the reservoir, a flux of material in the opposite direction towards the channel entrance occurred that partially removed the structured material. To avoid this, the suspension in the reservoir was removed after complete filling of the microchannels. Finally, the PDMS-mold was carefully removed from the CGO substrate as shown in Fig. 4e.

The described process was difficult to reproduce and turned out to be suitable only for prototyping of small electrochemical devices. The filling of microchannels is a statistical process so the filling length may vary considerably from channel to channel. Some of the cathode microchannels had been completely filled but most of them had not. This means that not all the electrodes were interdigitating. It was also observed that the anode microlines were always shorter than the cathode microlines, indicating that an increase of solid loading will decrease the average filling length, as already noticed by Heule et al. [17].

2.6.5. Sintering and electric contacting

The proposed electrode preparation process requires the co-sintering of the anode and cathode material (Fig. 4f). To ensure a good contact between the electrolyte and the anode and for obtaining a stable anode-microstructure a rather high sintering temperature of up to 1300 °C is required [20]. The cathode material should, however, not be sintered at temperatures above 1100 °C [19] because the microstructure becomes very coarse. Therefore, the cathode determines the maximum co-sintering

Table 2
Contact angle θ of water on PDMS and CGO-pellets before and after oxygen-plasma treatment

θ with PDMS before plasma cleaning	θ with PDMS after plasma cleaning	θ with CGO before plasma cleaning	θ with CGO after plasma cleaning
95	<7	65 ± 9.3	16 ± 1.7

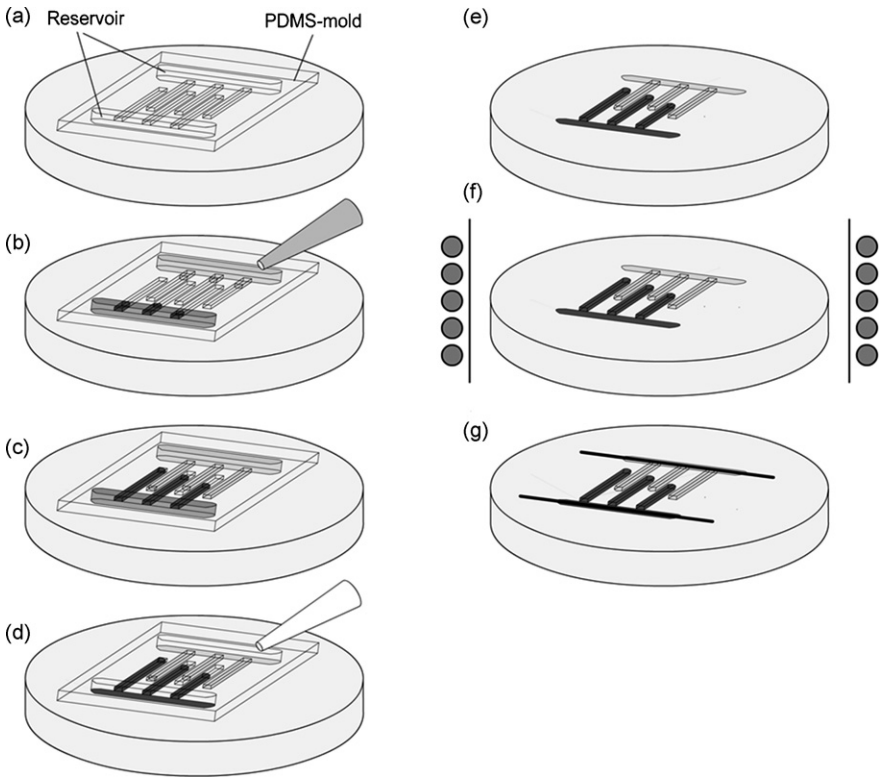

Fig. 4. Schematic of the MIMIC process for the preparation of micro-cells. (a) Place PDMS-mold on ion conducting CGO substrate, (b) apply suspension droplet in the reservoirs at the opening of the microchannels on each side of the mold, (c) capillary forces fill microchannels with anode and cathode suspensions from opposite sides of the PDMS-mold, (d) excess suspension is removed from the reservoirs and the microlines are slowly dried, (e) remove PDMS-mold: interdigitating array of anode and cathode stripes forming a micro-cell, (f) co-sinter both electrode arrays, (g) apply Pt-paste and flattened Pt-wire as current-collectors with subsequent heat treatment.

temperature, which was chosen to be at 1100 °C. The sintering was done in the same way as described in Section 2.4 with 2 h holding time at the peak temperature. The anodes and cathodes were connected as shown in Fig. 4g using Pt-paste (Heraeus C3605S) and flattened Pt-wire (Agar Scientific E404-1, 0.1 mm in diameter) at the beginning of the electrode arrays. First a layer of Pt-paste was screen-printed perpendicular to each electrode array where the reservoir was located during the MIMIC step. Then a Pt-wire was placed on top of each side of the cell. The Pt-paste/wire current-collectors were heat treated at 1100 °C for 1 h according to the instructions of the Pt-paste supplier. The Pt-wires were then fixed to the CGO substrate by refractory adhesive (Firag, Germany).

2.7. Connecting the Cells and electrochemical characterisation

The fabricated cells were heated to 650 °C in the test rig shown in Fig. 5. In this setup, the cell is supported in a round quartz glass holder and the gas flow comes from the top through a quartz glass tube in a centro-symmetrical configuration. The thermocouple (Type K) was placed very closely at the cells surface and was covered with a thin layer of refractory adhesive (Firag, Germany) in order to prevent erroneous temperature readings. Fuel cell tests were done at temperatures from 500 to 650 °C in methane–air mixtures with different CH_4/O_2 ratios (in the following denoted x). The total gas flow rate was varied from 100 to 300 ml min^{-1}. The voltage–current characteristics of the cell were obtained by a voltage sweep from the OCV to 0 V at a rate of 2–5 mV s^{-1} using a potentiostat (IM600, Zahner GmbH, Germany). This rate was found to be sufficiently low for allowing the cell to equilibrate during the whole measurement.

2.8. Comparison macro-, milli- and micro-cells

The characteristics of the different cells, such as total area of the cell, the electrode area, gap area, power density and specific power density are summarised in Table 3. The intra as well as intercellular spacings, the percentage of gap area of the whole cell area and the cell resistances, which were derived from the *U–I* curves, are also summarised. For obtaining the specific

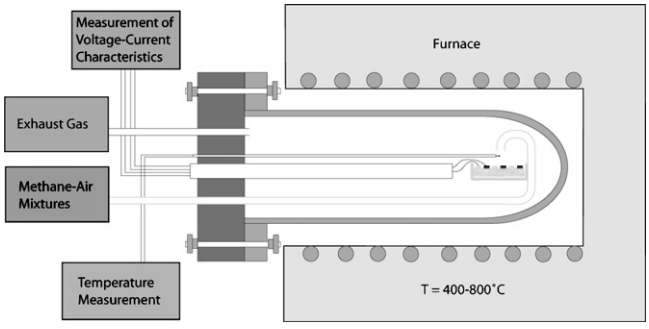

Fig. 5. SOFC test rig for the characterisation of the prepared SC-SOFCs.

Table 3
Characteristics of the prepared SC-SOFCs

	Macro-cell	Milli-cell	Micro-cell
Number of Cells	1	4	19
Area of cell (cm^2)	1.124	1.406	0.051
Electrode area (cm^2)	1.000	1.140	0.043
Gap area (cm^2)	0.124	0.266	0.005
Power density (mW)	2.1	2.05	0.86
Specific power density ($mW\,cm^{-2}$)	1.87	1.46	16.92
Intracellular spacing (m)	1.2×10^{-3}	3.6×10^{-4}	1.4×10^{-5}
Intercellular spacing (m)	–	4.5×10^{-4}	1.4×10^{-5}
Gap area (%)	11.0	18.9	9.0
Cell resistance (Ω)	71	51	164

power density, the measured power density was divided by the total cell area. The electrode area of the milli-cell was larger than 1 cm^2 because the paste spread from the edges after the screen-printing step. The nominal number of cells for the micro-cell was 46 with a total area of 1.011 cm^2. Because of the limitations of MIMIC by the statistic filling length of microchannels, not all the cells were active, i.e. with interdigitating electrodes. The micro-cell only had 19 active cells with a total area of 0.051 cm^2 (measured by light microscopy) of which only 9% were taken by intra and intercellular gaps.

3. Results

3.1. Macro-cell

The measured cell is shown in Fig. 6a before and Fig. 6b after the measurement. The green electrode (right) corresponds to the anode and the black electrode (left) to the cathode in Fig. 6a. A gap of 1.2 mm width separates the two electrodes both having a surface area of 0.5 cm^2. The Pt-mesh and wire can clearly be seen on both electrodes. In Fig. 6b, the cell is shown after the measurement. The anode had turned predominantly black due to the reduction of NiO to metallic Ni in the reducing CH_4–air mixtures, while the cathode showed no observable changes. Close to the gap, the anode material had turned white as a result of pronounced microstructural changes. SEM-micrographs of the unreduced anode and the black and white regions of the reduced anode are shown in Fig. 7. The unreduced anode (Fig. 7a) had a homogeneous, porous microstructure of NiO and CGO with a grain size of approximately 200 nm. The black area of the reduced anode far away from the gap (Fig. 7b) consisted of metallic nickel and CGO. The metallic phase is the reason why the material appears black and can clearly be distinguished from the ceramic CGO-grains. In the white region of the anode, very close to the gap, a loss of the metallic Ni was evidenced by SEM and also XRD, leaving behind a ruptured microstructure of CGO-grains (Fig. 7c). The CGO-particles still had the same size as in the black region but insufficient interconnectivity. The loss of metallic nickel was the cause for the change of colour from black to white. In Fig. 7d, a region in the white part is shown where metallic nickel had segregated to the surface of the anode layer. Volatilisation of Ni during the partial oxidation of methane at temperatures of around 730–830 °C is not an unknown phenomenon; Torniainen et al. [21] noticed the slow deactivation of monolith supported Ni-catalyst and could attribute this to the loss of Ni. They did not give an explanation how this loss occurred. As shown in previous work by Napporn et al. [22] a substantial overheating is caused at the anode by the presence of Pt-mesh. The magnitude of the overheating depends on the gas flow, the heating temperature and the mixing ratio of CH_4 and O_2. Thus, the temperature of the fuel cell could have easily reached temperatures above 700 °C, where the Ni-volatilisation was possible. Jacques-Bédard et al. reasoned that the loss of Ni in SC-SOFCs operating in CH_4–air mixtures could have been due to the formation of gaseous $Ni(OH)_2$ that was slowly but constantly removed by the incoming gas flow [23].

X-ray diffraction (XRD) measurements of the unreduced anode showed that the material was composed of NiO and CGO. The black region in the reduced anode (in Fig. 6b) indicated the presence of metallic Ni as well as some NiO, which was due to the superficial oxidation of the Ni-grains during the cooling of the fuel cell under CH_4–air mixture. The XRD-pattern

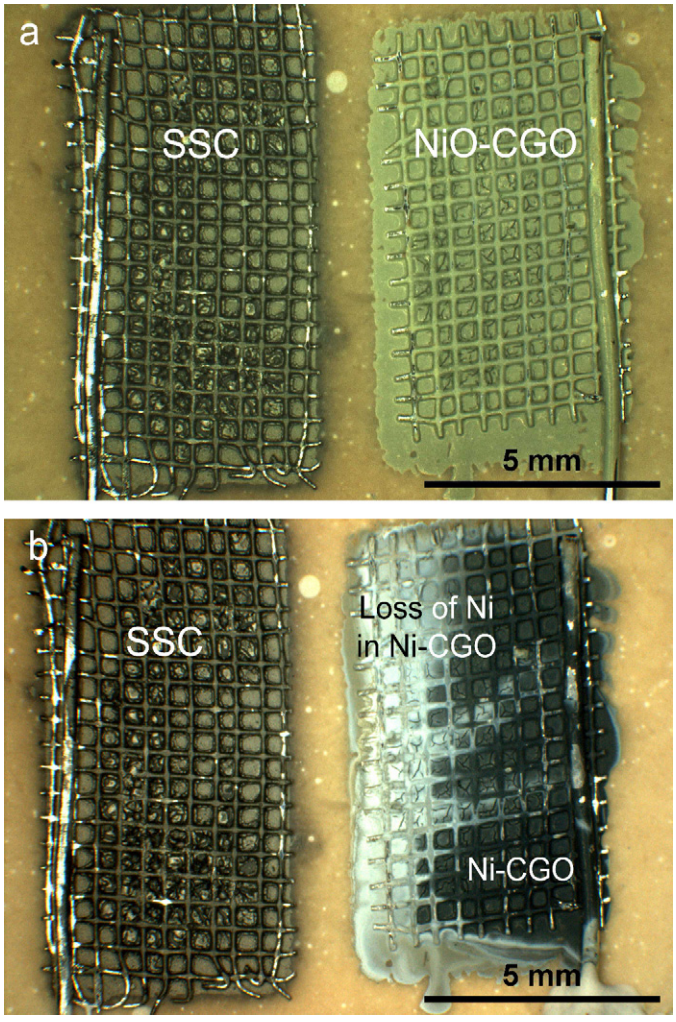

Fig. 6. Macro-cell (a) before and (b) after measurement in mixtures of CH_4 and air. The white region of the anode (left side) in (b) close to the gap was active while 60% of the electrode surface stays inactive. Pt-mesh and wire current-collectors were used for both electrodes.

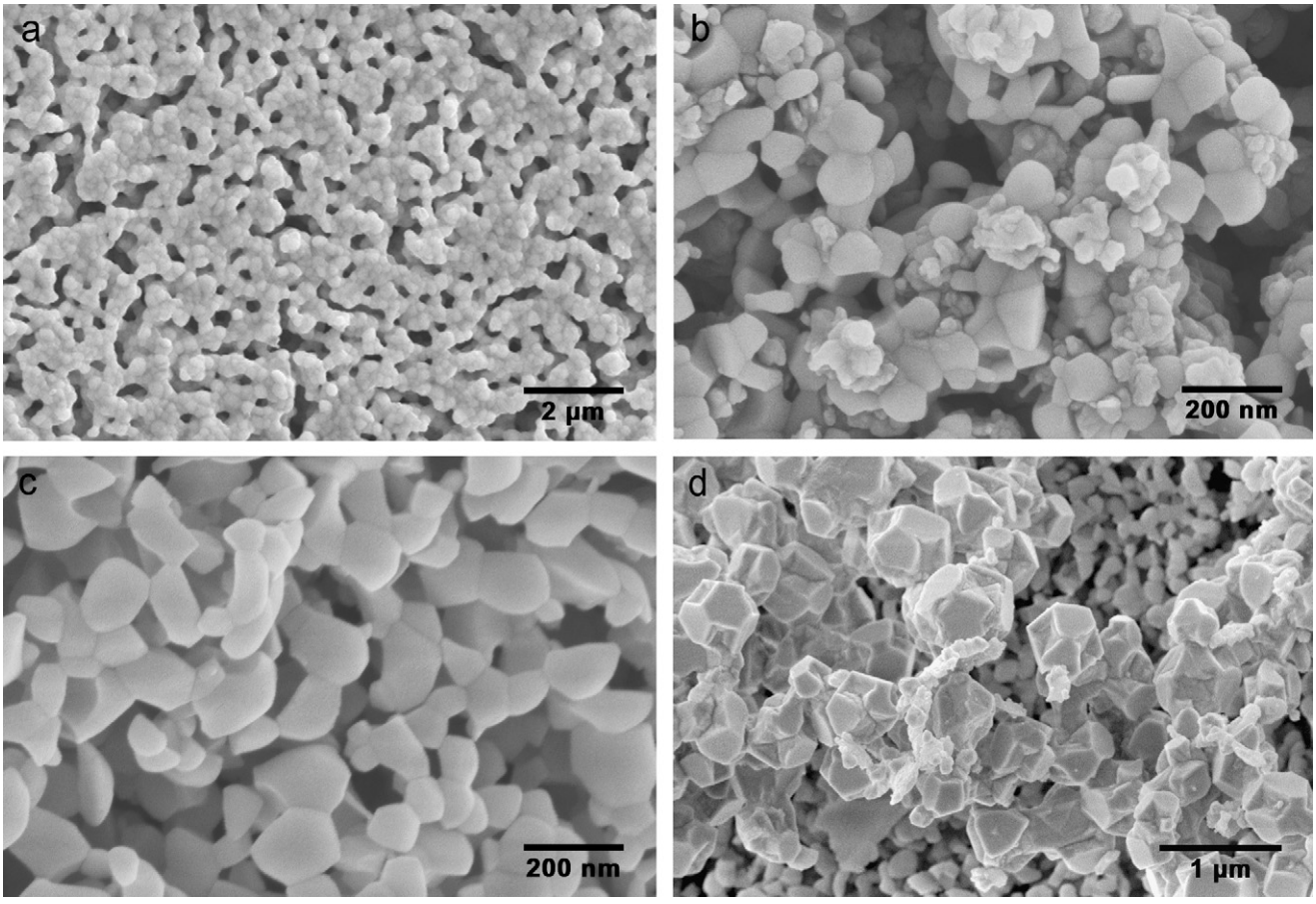

Fig. 7. SEM-micrographs showing the anode before (a) and after the measurement (b–d) of the macro-cell from Fig. 6. (a) The unreduced anode has a homogeneous, porous structure of NiO and CGO. (b) The anode structure in the black regions far away from the gap consists of metallic nickel and CGO-grains. (c) The anode structure in the white region very close to the gap corresponds to a region where the metallic phase was partially lost. (d) Ni-segregations on the surface of the anode material close to the gap.

of the white region showed the presence of CGO and some NiO but the peak for metallic nickel had become very small as compared to the same peak of the black region. This confirmed the Ni-loss that was already observed by use of a SEM. The observations suggest that only a small part of the anode close to the gap contributes to the fuel cell performance, while 60% of the surface area (black region) does not. The remote regions of both electrodes have long paths for the ionic current, which leads to high ohmic resistances. Therefore, the regions far away from the electrode gap stay inactive and it does not make sense to exceed a certain electrode width. In Fig. 8, the voltage–current characteristics of the macro-cell is shown at a temperature of 500 and 600 °C at $CH_4/O_2 = 3.2$. Under such conditions, the formation of carbon is thermodynamically possible as has been calculated in our recent work [24]. However, no carbon formation could be observed on the cell after the experiment neither on the electrolyte nor on the Pt current-collectors. CH_4 is not as prone to coking as the higher hydrocarbons. The increased temperature at the anode is another factor that prevents carbon formation. The OCV was close to 0.8 V for both temperatures, while the maximum power density reached 0.81 mW at 500 °C and 2.1 mW at 600 °C. Due to the very large gap size of 1.2 mm, the cell had a total resistance of 71 Ω at 600 °C.

3.2. Milli-cell

A digital photograph of the milli-cell with four parallel-connected cells is shown in Fig. 9. The average distance between

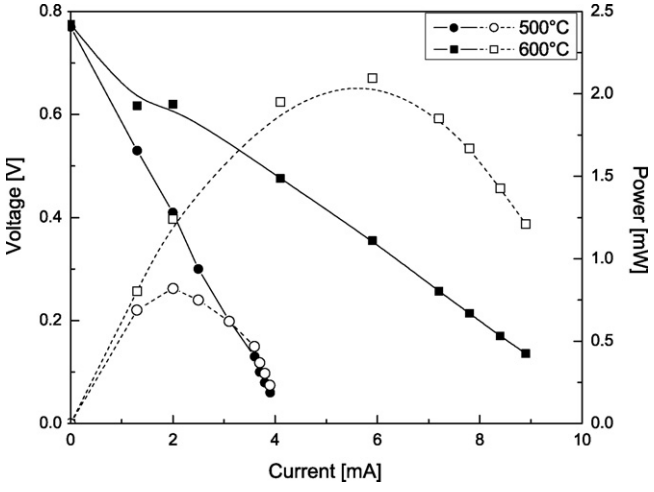

Fig. 8. Voltage–current characteristic of the macro-cell at a furnace temperature of 500 and 600 °C and a total flow rate of 125 ml min^{-1} CH_4–air mixture ($CH_4/O_2 = 3.2$).

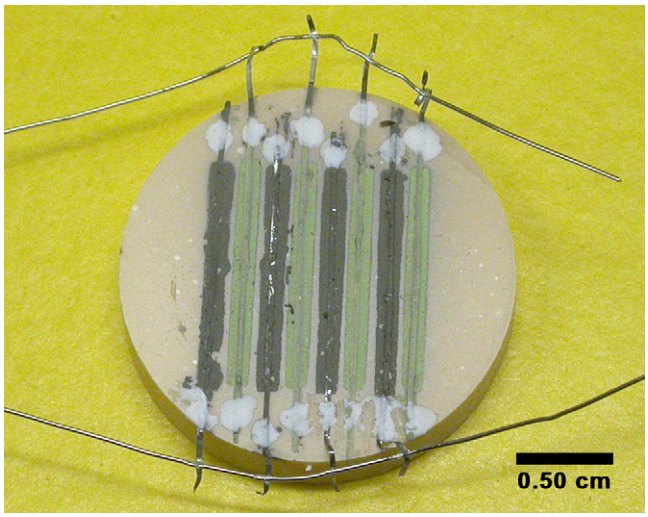

Fig. 9. Milli-cell: four parallel-connected SC-SOFCs on a CGO substrate. The Pt-wires used as current-collectors were attached to the electrolyte by small dots of refractory adhesive.

the two electrodes of one cell was 0.27 mm, between the electrodes of adjacent cells 0.36 mm. The total area of the cell was 1.41 cm^2. In Fig. 10, the voltage–current characteristic of the milli-cell is shown for different x-values (=CH_4/O_2) at 650 °C and 100 ml min^{-1} CH_4–air flow. The OCV reached a value of 0.72 V at $x = 1$ and 0.70 V at $x = 1.5$. When $x = 2$, the OCV was around 0.5 V and the cell behaviour was very unstable giving strongly fluctuating OCV. This is the reason why the voltage–current characteristic was not measured at these conditions. The maximum power output reached 1.18 mW at $x = 1.5$.

3.3. Micro-cell

In Fig. 11, a digital photograph of the prepared micro-cell is shown. Interdigitating microlines of anode and cathode materials only 100 μm wide were obtained by the modified MIMIC process. There was a statistical distribution of the final micro-

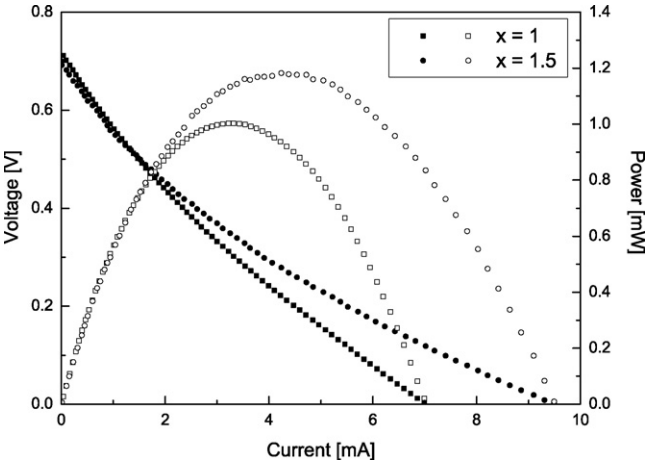

Fig. 10. Voltage–current characteristic of the fabricated milli-cell at different CH_4/O_2 ratios (x) at 650 °C with a total flow rate of 100 ml min^{-1} CH_4–air mixture. At $x = 2$, it was not possible to obtain a stable OCV, which is the reason why the voltage–current characteristic was not measured.

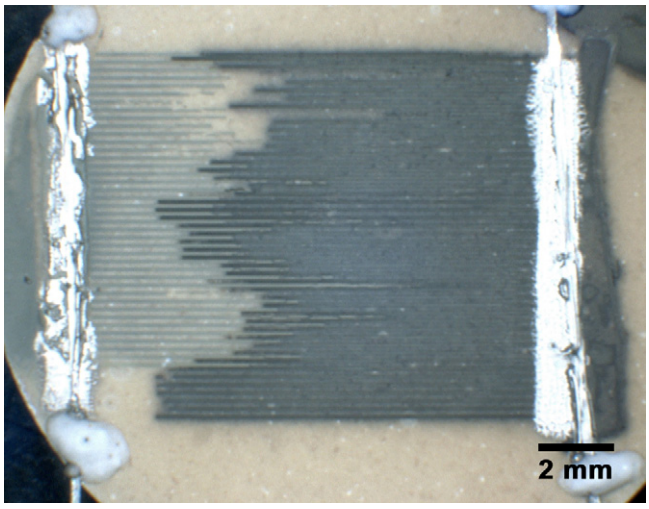

Fig. 11. Optical micrograph of the finished micro-cell prepared by MIMIC showing the cathode array (black), the anode array (grey), the electrolyte substrate, the Pt current-collectors as well as the refractory adhesive for fixing the Pt-wires to the electrolyte substrate.

line length as shown in Fig. 11, which was the reason why the electrodes were interdigitating only in a small region. Fig. 12 shows a SEM-micrograph of a region where the electrodes were interdigitating. The MIMIC process allowed the preparation of sub-millimetre electrodes that were separated by a very narrow gap of 14 μm. No cross-contamination of anode and cathode material was observed. The anode had a final width of 96.8 μm, while the cathode had a width of 91.4 μm. The initial width of the electrodes was 100 μm, the initial gap width 10 μm. This means that during the sintering step, there was a lateral shrinkage of 3.2% for the anode and 8.6% for the cathode. The high shrinkage of the cathode was accompanied by the formation of small cracks. The main reasons for this are the low solid loading of the MIMIC-suspension and the relatively high sintering temperature of 1100 °C. The gap width increased from an initial value of 10–14 μm. The electrodes were approximately 2–3 μm in height.

In Fig. 13, the voltage–current characteristic of the fabricated micro-cell is shown for a total flow rate of 100 ml min^{-1} of

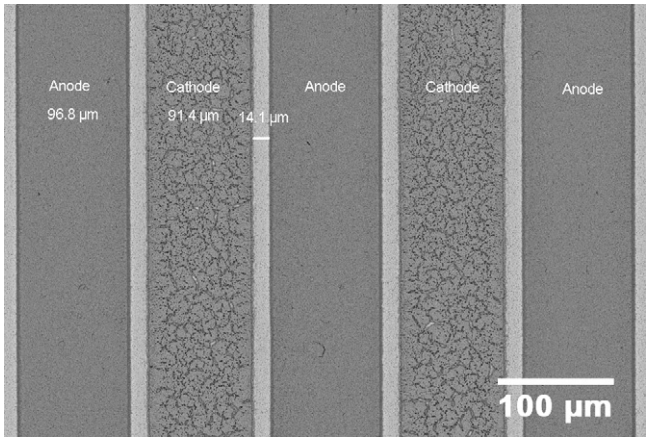

Fig. 12. Topview of a part of the active area of the micro-cell prepared by MIMIC.

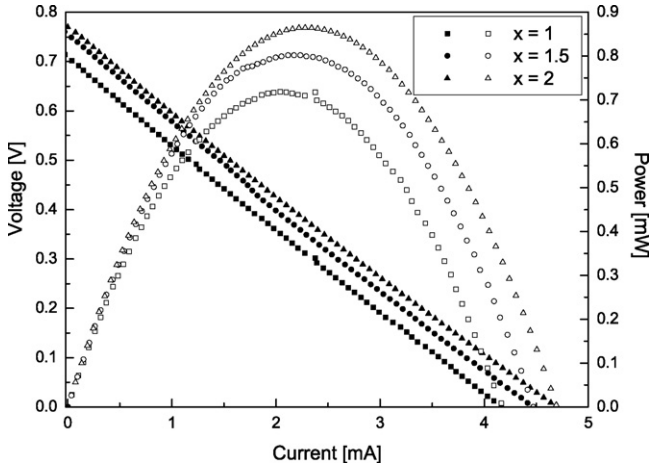

Fig. 13. Voltage–current characteristic of the fabricated micro-cell at different CH_4/O_2 ratios (x) at 650 °C with a total flow rate of 100 ml min^{-1} CH_4–air mixture.

CH_4–air mixtures with varying gas composition (x). The maximum power output was slightly higher than 0.86 mW. At 650 °C, the ohmic resistance of the cell was 164 Ω and the reason for this large resistance was due to the long conduction paths within the 100 μm wide and 3 μm thick electrodes to the active sites of the cell. The resistance of all anode and cathode strips was calculated to be around 23 and 70 Ω, respectively. It was found that the OCV as well as the maximum power output decreased when decreasing the x from 2 to 1, i.e. when using leaner gas mixtures. The reason for the decrease in OCV is likely to be due to the anode. In the ideal case, the cathode should be totally inert to the fuel. Therefore, at the cathode/electrolyte interface, an oxygen partial pressure equal to partial pressure in the gas phase should prevail. On the other hand, the anode should catalytically convert all the provided oxygen and produce a low $p(O_2)$ at the anode/electrolyte interface. However, in case of a very thin anode, a low oxygen partial pressure cannot be maintained. If more oxygen is fed to the anode surface than can be converted, the remaining oxygen will be present at the anode/electrolyte

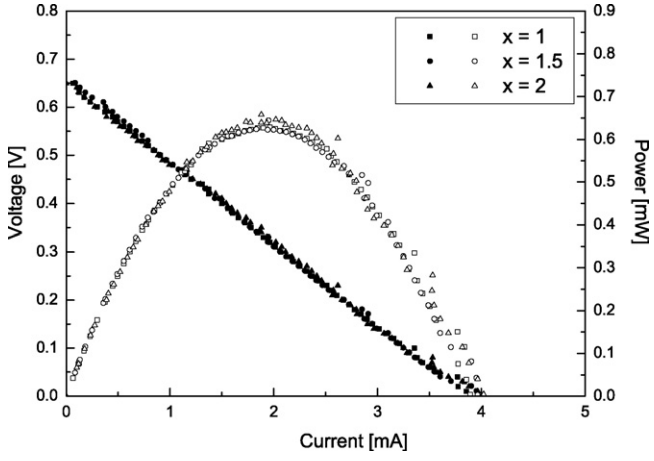

Fig. 14. Voltage–current characteristic of the fabricated micro-cell for different CH_4/O_2 ratios (x) at 650 °C with a total flow rate of 300 ml min^{-1} CH_4–air mixture.

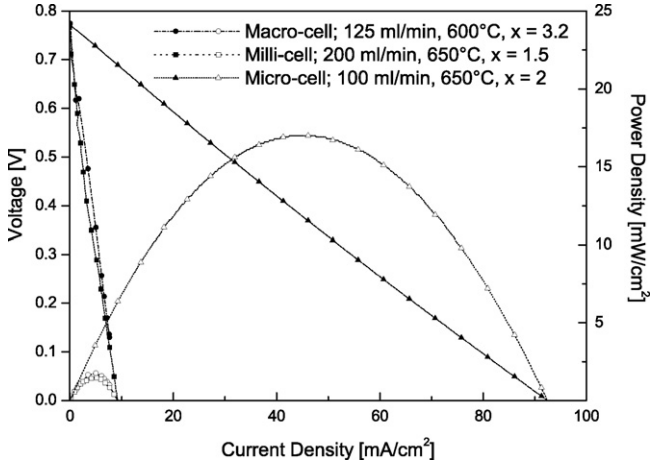

Fig. 15. Voltage–current characteristics of the prepared side by side SC-SOFCs normalised to the cell area including inter and intracellular gaps.

interface. This lowers the chemical potential difference and therefore OCV, as observed with $x = 1$. Consequently, if the flow rate of gas mixture increases, the OCV should decrease. In fact, when the flow rate was increased to 300 ml min^{-1} (see Fig. 14), the OCV was no longer a function of x and the absolute value was 0.65 V, which was lower than the value at 100 ml min^{-1}. The maximum power output also decreased to about 0.6 mW.

3.4. Comparison of macro-, milli- and micro-cells electrochemical performances

The prepared cells are compared in Fig. 15 at the conditions yielding the highest power output. All the cells had an OCV between 0.70 and 0.77 V. The macro- and milli-cells had a similar power output of around 1.5 mW cm^{-2} at the given conditions. For the milli-cell, a higher OCV was measured at $x = 1$ as compared to $x = 1.5$. In contrast, the power output showed the opposite trend, i.e. the performance at $x = 1$ was lower than at $x = 1.5$ (see Fig. 10). As can be seen in Fig. 13, the OCV of the micro-cell decreased with decreasing x-value, which corresponds to the behaviour of the milli-cell. The micro-cell with an active area of 0.051 cm^2 showed the highest specific power output of 17 mW cm^{-2} at 650 °C. As was shown in Fig. 14, the power maximum power output of the micro-cell was obtained at $x = 2$ where also the highest OCV was measured.

4. Discussion

The OCVs of the screen-printed macro- and milli-cells are mainly determined by the thick cathode layer. As the oxygen partial pressure in the initial gas mixture is increased, the OCV is also raised. The oxygen partial pressure at the anode–electrolyte interface does not strongly depend on the initial gas mixture because the thickness of the catalytic layer is large enough to remove most of the molecular oxygen from the gas mixture before it reaches the interface even at a high flow rates. In contrast, the OCV of the micro-cell is mainly determined by the thin anode layer, which catalyses the partial oxidation reaction that

removes the oxygen before it can reach the anode–electrolyte interface. The higher the oxygen partial pressure in the initial gas phase the more oxygen will penetrate to the anode–electrolyte interface through the thin anode layer thereby decreasing the measured OCV.

The results presented in Fig. 15 demonstrate that it is possible to improve the area specific power density of side by side SC-SOFCs by reducing the gap width between the anode and the cathode of an individual cell. In order to minimise the inactive area of the electrodes at the far side of each gap, the electrode width must also be reduced. A drastic reduction of the OCV by an increased electronic current in the CGO electrolyte was not observed. Furthermore, a reduction of the OCV by the diffusion of H_2 and CO from the anode to the cathode could also be ruled out by OCV-values higher than 0.7 V. Alternating electrodes of anode and cathode materials were fabricated by using closed end capillaries in PDMS-molds. These were filled by capillary action from opposite sides with suspensions of both electrode materials. Not all the capillaries could be completely filled and only an incomplete array of cells was formed with electrodes that were interdigitating only in certain regions. The described MIMIC-process yielded cells, which were connected in parallel by the deposited material, where the reservoir of the MIMIC step was located. Despite the possibility of hydrogen and carbon monoxide from the anode reaching the cathode a high OCV of 0.70 V at $x = 1.1$ and 650 °C could be obtained. The OCV was comparable to the value obtained by Hao et al. for ceria-based cells with electrodes on either side of the electrolyte [25]. This proves that the concept of a micro-cell with a side by side placement of electrodes is feasible. Series connection of cells would make the array of cells more flaw-tolerant, because cracks perpendicular to the electrodes cannot block the current coming from beyond this point of the electrode. In addition the excessive ohmic resistance due to the long conduction path within the very narrow and flat electrodes from the current-collector to the active sites, i.e. where the electrodes were interdigitating could be avoided. However, for a series-connection of the cells, interconnect strips are needed and the preparation of the latter requires an additional processing step with an exact alignment. The large number of cells for the micro-cell and the possibility of easy series interconnection make it possible to obtain useful voltages without the need for constructing a fuel cell stack. Furthermore, it will not be necessary to have a current-collector for every electrode because the voltage drop across the width of one electrode will be very small due to the short distance of the conducting path. Thus, for micro-cells, we propose the series-connection of cells. The required voltage can be adjusted by the number of cells, the envisaged power output by the choice of the appropriate electrode length. The electrolyte ohmic resistance can be decreased by decreasing the gap width between anode and cathode. However, the minimum gap width can be expected to be at around 0.3 μm because then the local field strength of $3 \times 10^6\ \mathrm{V\,m^{-1}}$ will be approached, which corresponds to the breakdown voltage in air [1].

The advantage of the micro-cells is that the gap area between the electrodes is very small as compared to normal cells, which leads to a better utilisation of the surface area.

5. Conclusions

Micro-single chamber solid oxide fuel cells were fabricated by micromolding in capillaries of electrodes on CGO electrolytes. The described process was difficult to reproduce and turned out to be suitable only for prototyping of small electrochemical devices. The reason for this is that the filling of the capillaries is a statistical process and that the resulting structures were difficult to dry. It would be advisable to find a more powerful preparation procedure that yields micro-cells with complete electrode arrays. Nevertheless, this work clearly showed that micro-cells could operate in CH_4–air mixture giving them a great potential in terms of area-specific performance for applications where portable miniaturised solid oxide fuel cells systems are needed.

Acknowledgements

The authors would like to thank Lars Massüger for the help with the XRD-analysis with thin quartz glass capillaries and Dr. Marc Dusseiller for contributing some of the figures.

References

[1] W. van Gool, Philips Res. Rep. 20 (1965) 81–93.
[2] G.A. Louis, J.M. Lee, D.L. Maricle, J.C. Trocciola, US Patent 4,248,941 (1981).
[3] T. Hibino, H. Iwahara, Chem. Lett. 7 (1993) 1131–1134.
[4] T. Hibino, K. Ushiki, T. Sato, Y. Kuwahara, Solid State Ionics 81 (1995) 1–3.
[5] T. Hibino, H. Tsunekawa, S. Tanimoto, M. Sano, J. Electrochem. Soc. 147 (2000) 1338–1343.
[6] T. Hibino, A. Hashimoto, S. Masanori, Y. Masaya, Y. Shin-ichiro, S. Mitsuru, J. Electrochem. Soc. 149 (2002) A195–A200.
[7] T. Matsui, M. Inaba, A. Mineshige, Z. Ogumi, Solid State Ionics 176 (2005) 647–654.
[8] T. Hibino, K. Ushiki, Y. Kuwahara, Solid State Ionics 91 (1996) 69–74.
[9] J. Fleig, H.L. Tuller, J. Maier, Solid State Ionics 174 (2004) 261–270.
[10] C.-Y. Chung, Y.-C. Chung, J. Power Sources 154 (2006) 35–41.
[11] T. Hibino, A. Hashimoto, M. Yano, M. Suzuki, S.-I. Yoshida, S. Mitsuru, J. Electrochem. Soc. 149 (2002) A133–A136.
[12] Y. Xia, G.M. Whitesides, Angew. Chem. Int. Ed. 37 (1998) 550–575.
[13] Y. Xia, G.M. Whitesides, Annu. Rev. Mater. Sci. 28 (1998) 153–184.
[14] U.P. Schönholzer, L.J. Gauckler, Adv. Mater. 11 (1999) 630–632.
[15] U.P. Schönholzer, R. Hummel, L.J. Gauckler, Adv. Mater. 12 (2000) 1261–1263.
[16] M. Heule, L.J. Gauckler, Sens. Actuators B 93 (2003) 100–106.
[17] M. Heule, J. Schell, L.J. Gauckler, J. Am. Ceram. Soc. 86 (2003) 407–412.
[18] S.G. Charati, S.A. Stern, Macromolecules 31 (1998) 5529–5535.
[19] B.E. Buergler, M.E. Siegrist, L.J. Gauckler, Solid State Ionics 176 (2005) 1717–1722.
[20] R. Maric, S. Ohara, T. Fukui, T. Inagaki, J.-I. Fujita, Electrochem. Solid-State Lett. 1 (1998) 201–203.
[21] P.M. Torniainen, X. Chu, L.D. Schmidt, J. Catal. 146 (1994) 1–10.
[22] T.W. Napporn, F. Morin, M. Meunier, Electrochem. Solid-State Lett. 7 (2004) A60–A62.
[23] X. Jacques-Bedard, T.W. Napporn, R. Roberge, M. Meunier, J. Power Sources 153 (2006) 108–113.
[24] B.E. Buergler, A.N. Grundy, L.J. Gauckler, J. Electrochem. Soc. 153 (2006) A1378–A1385.
[25] Y. Hao, Z. Shao, J. Mederos, W. Lai, D.G. Goodwin, S.M. Haile, Solid State Ionics 177 (2006) 2013–2021.